NASA/TM—2018-219885

The Effectiveness of a NiCrY-Coating on a Powder Metallurgy Disk Superalloy

Timothy P. Gabb
Glenn Research Center, Cleveland, Ohio

Robert A. Miller
Vantage Partners, LLC, Brook Park, Ohio

James A. Nesbitt, Susan L. Draper, Richard B. Rogers, and Jack Telesman
Glenn Research Center, Cleveland, Ohio

April 2018

NASA STI Program . . . in Profile

Since its founding, NASA has been dedicated to the advancement of aeronautics and space science. The NASA Scientific and Technical Information (STI) Program plays a key part in helping NASA maintain this important role.

The NASA STI Program operates under the auspices of the Agency Chief Information Officer. It collects, organizes, provides for archiving, and disseminates NASA's STI. The NASA STI Program provides access to the NASA Technical Report Server—Registered (NTRS Reg) and NASA Technical Report Server—Public (NTRS) thus providing one of the largest collections of aeronautical and space science STI in the world. Results are published in both non-NASA channels and by NASA in the NASA STI Report Series, which includes the following report types:

- TECHNICAL PUBLICATION. Reports of completed research or a major significant phase of research that present the results of NASA programs and include extensive data or theoretical analysis. Includes compilations of significant scientific and technical data and information deemed to be of continuing reference value. NASA counter-part of peer-reviewed formal professional papers, but has less stringent limitations on manuscript length and extent of graphic presentations.

- TECHNICAL MEMORANDUM. Scientific and technical findings that are preliminary or of specialized interest, e.g., "quick-release" reports, working papers, and bibliographies that contain minimal annotation. Does not contain extensive analysis.

- CONTRACTOR REPORT. Scientific and technical findings by NASA-sponsored contractors and grantees.

- CONFERENCE PUBLICATION. Collected papers from scientific and technical conferences, symposia, seminars, or other meetings sponsored or co-sponsored by NASA.

- SPECIAL PUBLICATION. Scientific, technical, or historical information from NASA programs, projects, and missions, often concerned with subjects having substantial public interest.

- TECHNICAL TRANSLATION. English-language translations of foreign scientific and technical material pertinent to NASA's mission.

For more information about the NASA STI program, see the following:

- Access the NASA STI program home page at http://www.sti.nasa.gov

- E-mail your question to help@sti.nasa.gov

- Fax your question to the NASA STI Information Desk at 757-864-6500

- Telephone the NASA STI Information Desk at 757-864-9658

- Write to:
  NASA STI Program
  Mail Stop 148
  NASA Langley Research Center
  Hampton, VA 23681-2199

NASA/TM—2018-219885

The Effectiveness of a NiCrY-Coating on a Powder Metallurgy Disk Superalloy

Timothy P. Gabb
Glenn Research Center, Cleveland, Ohio

Robert A. Miller
Vantage Partners, LLC, Brook Park, Ohio

James A. Nesbitt, Susan L. Draper, Richard B. Rogers, and Jack Telesman
Glenn Research Center, Cleveland, Ohio

National Aeronautics and
Space Administration

Glenn Research Center
Cleveland, Ohio 44135

April 2018

Acknowledgments

The authors would like to acknowledge the hard work of Dr. Ronghua Wei at Southwest Research Institute for coating the specimens, Don Humphrey and John Setlock of Zin Technologies, Inc. for heat treating the specimens. Dr. James Smialek is acknowledged for numerous helpful discussions, and Dr. Ivan Locci is acknowledged for reviewing this manuscript. This work was sponsored by the Advanced Air Transport Technology Program at the NASA Glenn Research Center.

Level of Review: This material has been technically reviewed by technical management.

Available from

NASA STI Program
Mail Stop 148
NASA Langley Research Center
Hampton, VA 23681-2199

National Technical Information Service
5285 Port Royal Road
Springfield, VA 22161
703-605-6000

This report is available in electronic form at http://www.sti.nasa.gov/ and http://ntrs.nasa.gov/

The Effectiveness of a NiCrY-Coating on a Powder Metallurgy Disk Superalloy

Timothy P. Gabb
National Aeronautics and Space Administration
Glenn Research Center
Cleveland, Ohio 44135

Robert A. Miller
Vantage Partners, LLC
Brook Park, Ohio 44142

James A. Nesbitt, Susan L. Draper, Richard B. Rogers, and Jack Telesman
National Aeronautics and Space Administration
Glenn Research Center
Cleveland, Ohio 44135

Abstract

Protective ductile coatings could be necessary to mitigate oxidation and corrosion attack on superalloy disks in some turbine engine applications. However, the effects of coatings on fatigue life of the disk during service are an important concern. The objective of this study was to investigate how such a coating could perform after varied post-coating processing. Cylindrical gage fatigue specimens of powder metallurgy-processed disk superalloy LSHR were coated with a NiCrY coating, shot peened, preparation treated, exposed, and then subjected to fatigue at high temperature. The effects of varied shot peening, preparation treatment, and exposures on fatigue life with and without the coating were compared. Each of these variables and several of their interactions significantly influenced fatigue life.

Introduction

Disk application temperatures of 700 °C and higher can enhance oxidation and also activate hot corrosion attack modes in harmful environments. These damage modes could become important design limitations (Ref. 1).

Several studies have shown that oxidation from exposures at 700 °C and higher can impair the fatigue resistance of disk superalloys (Refs. 2 and 3). This oxidation encompassed the formation of oxide layers and changes in superalloy chemistry and phases adjacent to the oxide layers. While the formation of chromium oxide is known to be protective, other nickel, cobalt, and titanium oxides can also form that are considered nonprotective. In addition, selective oxidation of certain elements can result in the formation of a zone adjoining the oxide layers of weakened gamma phase without gamma prime precipitates, which can be recrystallized to a finer grain size than the original disk alloy grains. The grain boundaries in this zone can be susceptible to cracking during fatigue at high temperatures, due in part to a lack of $M_{23}C_6$ carbides (Ref. 4). Collectively, these features can lower the mechanical fatigue resistance at the surface of disk superalloys.

Type II hot corrosion attack can occur at 700 °C to nearly 800 °C on superalloy surfaces (Refs. 5 and 6) by the melting of accumulated deposits containing mixtures of sodium-, magnesium-, and calcium-sulfates, as well as by direct impingement of SO_2-containing exhaust gas. However, SO_2 gas is not necessary for hot corrosion attack by these deposits. Here, the liquid sulfates can react with surface oxides to make them no longer protective. This allows penetration of the newly exposed superalloy surface. The attack can be further enhanced at the grain boundaries in superalloys for certain conditions. Pits can form

in some conditions, while general corrosion can otherwise occur (Ref. 7). The pits can act as geometric stress concentration sites, which encourage cracks to initiate during mechanical fatigue loading. Pitting and uniform corrosion can significantly reduce the fatigue resistance of disk superalloys (Refs. 3, 8 to 11).

For susceptible locations, a suitable metallic coating could provide protection of exposed disk surfaces from this oxidation and corrosion for relevant temperatures and environments. PtAl, NiAl, and NiCoCrAlY (Ref. 12) coatings have been extensively developed to protect superalloy airfoils from oxidation and corrosion. These coatings have also been used to serve as "bond coatings" between the superalloy and thermal barrier coatings. However, many of these coatings have lower ductility and fatigue resistance than turbine disk superalloys, for likely turbine disk temperatures extending up to 760 °C. Yet, simple early NiCr coatings were capable of forming a Cr_2O_3 coating that could be protective at disk application temperatures, while presumably still remaining ductile. A suitable ductile coating would have minimal effects on the fatigue resistance of the disk surfaces upon which it is applied, as disks are fatigue-limited and fracture critical in aero-propulsion applications.

Many machined surfaces of turbine disks are subsequently shot peened. This is because shot peening can produce a consistent surface finish and impart beneficial compressive residual stresses near the treated surfaces, that can impede fatigue cracking there (Refs. 14 and 15). A protective coating could be applied after fully machining a disk surface location, and before shot peening. The disk including its coated surfaces could then be shot peened. The residual stresses, roughness, and fatigue life before and after exposures of such coated and shot peened surfaces would need to be considered for such an approach, in order to balance the coating's effect on the disk's resistance to fatigue cracking with protection from oxidation and corrosion attack.

The objective of the study was to determine the effects of a ductile NiCrY coating on fatigue life of a powder metallurgy disk superalloy. The effects of post-coating processing including shot peening, heat treatment, and exposures on residual stresses, roughness, and fatigue life were evaluated.

Materials and Procedure

The powder metallurgy disk superalloy LSHR test material had the composition listed in weight percent of 3.54Al-0.027B-0.045C-20.4Co-12.3Cr-0.1Fe-2.71Mo-1.49Nb-0.02O-0.012Si-1.52Ta-3.45Ti-0.01V-4.28W-0.049Zr-balance Ni. LSHR superalloy powder had been atomized in argon, consolidated by hot isostatic pressing, extruded, and then segments were isothermally forged into flat disks (Ref. 16). Rectangular blanks about 13 mm square and 66 mm to 83 mm long were extracted from the as-forged disks. These blanks were each consistently supersolvus solution heat treated at 1171 °C for 2 h and subsequently aging heat treated at 855 °C for 4 h, followed by 775 °C for 8 h. The resulting LSHR microstructure had an average linear intercept grain size of about 15 μm, as shown after etching in Waterless Kalling's etchant in Figure 1(a). Fatigue specimens having uniform gage sections 6.4 mm in diameter were then machined to the dimension shown in Figure 2. These test specimens were all machined by low stress grinding, followed by longitudinal polishing (LP) with abrasive paper to a root mean square roughness of less than 0.2 μm.

High Power Impulse Magnetron Sputtering (HiPIMS) was employed by Southwest Research Institute to apply a Ni-45Cr-0.15Y (weight percent, nominal) coating. Prior to coating, the gage surface of each specimen to be coated was prepared by grit blasting using alumina grit at a pressure of 585 kPa (85 psi). Both ends of each specimen were masked with metal foil so that only the reduced gauge test section was exposed for coating. Each specimen was attached to a planetary rotating fixture to enable production of a uniform coating thicknesses on the individual samples. Five specimens were thereby coated during a single coating run. Three coating runs were made under identical run conditions.

The typical microstructure of the coating after application and subsequent shot peening and specimen preparation treatment is shown in Figures 1(b) to (d). The coating had a mean thickness of 26.5 μm with a 95% confidence interval of ±1.3 μm, using measurements of sections from unexposed test specimens. It consisted of a γ nickel-rich matrix with about 15 area percent of α chromium-rich precipitates. The α

precipitates had a wide range of sizes, with equivalent radius extending from 0.01 to 0.31 μm (Figs. 1(c) and (d)). Embedded alumina grit particles from the grit blasting are evident at the coating/substrate interface (Fig. 1(c)). The effect of the rough grit blast surface can also be seen at the coating/substrate interface in a later section (Fig. 14).

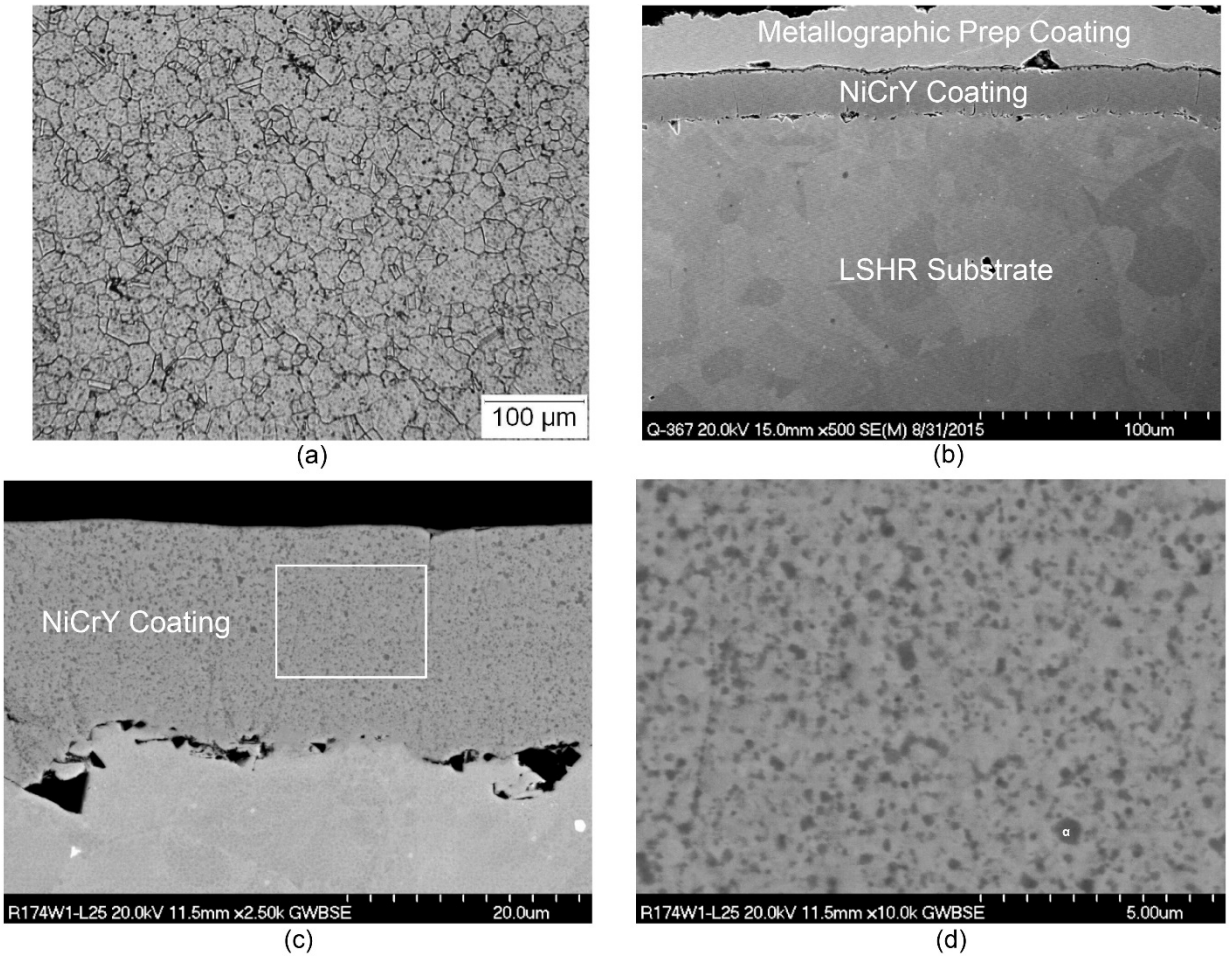

Figure 1.—Microstructures of (a) LSHR powder metallurgy disk superalloy with an average linear intercept grain size of about 15 μm, (b) coating at low magnification, (c) back-scattered election image of the coating on the surface of the LSHR substrate. Embedded alumina grit particles from the grit blasting are evident at the coating/substrate interface. (d) Higher magnification of the coating (inset in c) showing the α-Cr particles (dark).

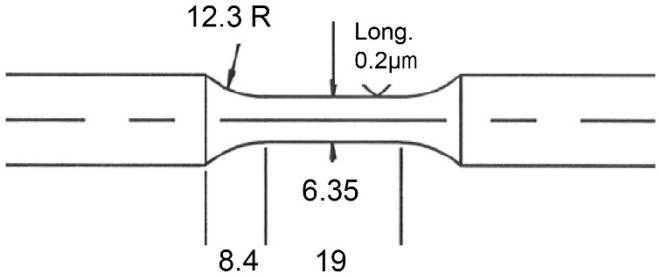

Figure 2.—Fatigue specimen with dimensions in mm.

Uncoated and coated fatigue test specimens were given varied shot peening, specimen preparation treatment atmosphere, and environmental exposures before fatigue testing. Coated and uncoated fatigue test specimens were first shot peened at Curtiss-Wright, Metal Improvement Division using conditioned cut stainless steel wire (CCW14). Two combinations of intensity and coverage were applied: (a) low intensity and coverage (4 N-100%), and (b) higher intensity and coverage (16 N-200%). Here, 100% coverage indicates 100% of the surface area has been impacted, while 200% indicates 200% of the time of shot peening needed to attain this 100% of coverage (Ref. 17).

After shot peening, all test specimens were given a specimen preparation treatment of 760 °C for 8 h in either atmospheric air or a low oxygen partial pressure to help form a protective chromium-oxide layer on the surface, and for the coated specimens, to promote interdiffusion between the coating and substrate. At atmospheric pressure, both protective Cr_2O_3 and nonprotective NiO oxides can form. Yet the applied low partial pressure of oxygen that was calculated to be 1×10^{-16} MPa (Ref. 18) equaled the equilibrium oxygen pressure for the formation of NiO, which allowed Cr_2O_3 formation but not NiO. This low pO_2 was achieved using ultra high purity Ar and large surface areas of high purity Ni foil. Lab air was used as the high pressure oxygen with a partial pressure of oxygen of 0.021 MPa.

A subset of coated and uncoated specimens was then also given environment exposures to oxidation, hot corrosion, or oxidation followed by hot corrosion. Oxidation was performed in lab air at 760 °C for 500 h. Hot corrosion treatments were also performed in lab air, by first coating specimens with a salt mixture of 69 wt% Na_2SO_4 and 31 wt% $MgSO_4$ (72 mol.% Na_2SO_4 – 28 mol.% $MgSO_4$) applied at 2 mg/cm^2. They were then suspended horizontally in a resistance-heating tube furnace at 760 °C for 50 h. This salt composition lies on the Na_2SO_4 side of the eutectic composition (melting point of 662 °C) but was observed to melt and flow in previous testing at 760 °C. This is in agreement with the Na_2SO_4-$MgSO_4$ phase diagram (Ref. 19). Previous work demonstrated that uncoated LSHR test specimens treated in this manner and tested at 760 °C in air nucleated and grew corrosion pits within just 24 h, which had a substantial effect on fatigue lives (Ref. 20). Coated and uncoated fatigue specimens which were given this corrosion for 50 h were again examined in the SEM for the presence of pits.

In order to obtain more useful statistical results, each variable was treated as continuous. Coating thickness in units of microns was used for coating (C), shot peening intensity in units of N was used for shot peening (SP), logarithm of the partial pressure of oxygen (LP) was used for the specimen preparation treatment, oxidation time in hours was used for oxidation (O) exposure, and hot corrosion time in hours was used for hot corrosion (HC) exposure. For regression modeling, each of these variables (V) was normalized to have values (V') between –1 and +1 using the equation:

$$V' = (V - V_{mid})/(\Delta V/2)$$

A half-factorial design of experiments was employed to screen the effects of these variables (Ref. 21), using two levels for each of these five variables (2^{5-1}). This design would allow estimates of the linear effect of each variable, as well as the effect of the 2-way interactions of each variable. To select the experiments, the product of the normalized variables for each possible combination of settings was calculated as shown in Table 1, and the cases in which this product was +1 were selected for testing. This gave the 16 combinations listed in Table 2, which were selected out of the 32 possible combinations. The resulting tabulated conditions for each of the 16 selected experiments are listed in Table 3. Duplicate specimens and fatigue tests were run for each selected experiment for a total of 32 tested specimens.

Fatigue cycling was conducted using a servo-hydraulic test machine with a resistance heating furnace integrated to enclose the specimen and specimen grips. Stress was consistently cycled between maximum and minimum stress values of 841 MPa and –427 MPa in each cycle using a saw-tooth waveform at a frequency of 0.33 Hz. These stresses corresponded to the stabilized maximum and minimum stresses produced by tests run on this material with strain cycled at a strain range of 0.76% and strain ratio (minimum/maximum strain) of 0 at 760 °C. However, in the present tests stress was cycled, and an extensometer was not used to contact the coated specimen surface for measuring strain, to avoid harming the coating.

Selected coated and uncoated fatigue specimens were examined before and after shot peening, after heat treatment at 760 °C for 8 h, and after exposures. All test specimen fracture surfaces were later examined after fatigue cycling to failure. Residual stresses were measured on the gage surface before fatigue testing using a Bruker D8 Discover (area detector) x-ray diffractometer aligned in accordance with the approach and error bounds specified in ASTM E 915-10, but applied to the side-inclination rather than iso-inclination method. Data was gathered using Mn Kα radiation and the (311) crystallographic plane on a specimen target area of 1.2 mm^2 (Ref. 22). These x-ray results were analyzed using the Bruker LEPTOS v.7 software. Peak width was measured using the Bruker TOPAS program. Average roughness (Ra) was measured using an Alicona InfiniteFocus G4 3D optical measurement system, with a 5x objective lens magnification giving a resolution of 0.41 μm. Gage and fracture surfaces were examined using a JEOL 6100 scanning electron microscope (SEM). The profiles of notable features on the gage sides of specimens were estimated using the Alicona MeX image metrology software package with stereo pair images taken with the SEM. Actual coating thickness was measured adjacent to the dominant crack causing failure on unexposed coated fatigue specimens' fracture surfaces. Sections transverse and parallel to the axial loading direction were metallographically prepared from the gage of selected fatigue specimens, for examination with an optical microscope as well as a SEM.

TABLE 1.—ALL COMBINATIONS OF STANDARDIZED VARIABLES, AND THEIR RESULTING PRODUCT. THE COMBINATIONS HAVING A RESULTING PRODUCT OF 1 WERE SELECTED FOR TESTING

Coating	Shot Peening	Oxygen Partial Pressure	Oxidation	Corrosion	***Product***
-1	-1	-1	-1	-1	***-1***
-1	-1	-1	-1	1	***1***
-1	-1	-1	1	-1	***1***
-1	-1	-1	1	1	***-1***
-1	-1	1	-1	-1	***1***
-1	-1	1	-1	1	***-1***
-1	-1	1	1	-1	***-1***
-1	-1	1	1	1	***1***
-1	1	-1	-1	-1	***1***
-1	1	-1	-1	1	***-1***
-1	1	-1	1	-1	***-1***
-1	1	-1	1	1	***1***
-1	1	1	-1	-1	***-1***
-1	1	1	-1	1	***1***
-1	1	1	1	-1	***1***
-1	1	1	1	1	***-1***
1	-1	-1	-1	-1	***1***
1	-1	-1	-1	1	***-1***
1	-1	-1	1	-1	***-1***
1	-1	-1	1	1	***1***
1	-1	1	-1	-1	***-1***
1	-1	1	-1	1	***1***
1	-1	1	1	-1	***1***
1	-1	1	1	1	***-1***
1	1	-1	-1	-1	***-1***
1	1	-1	-1	1	***1***
1	1	-1	1	-1	***1***
1	1	-1	1	1	***-1***
1	1	1	-1	-1	***1***
1	1	1	-1	1	***-1***
1	1	1	1	-1	***-1***
1	1	1	1	1	***1***

TABLE 2.—ALL COMBINATIONS OF STANDARDIZED VARIABLES GIVING A PRODUCT OF 1, THE CASES WHICH WERE SELECTED FOR TESTING

Coating	Shot Peening	Oxygen Partial Pressure	Oxidation	Corrosion	**Product**
-1	-1	-1	-1	1	***1***
-1	-1	-1	1	-1	***1***
-1	-1	1	-1	-1	***1***
-1	-1	1	1	1	***1***
-1	1	-1	-1	-1	***1***
-1	1	-1	1	1	***1***
-1	1	1	-1	1	***1***
-1	1	1	1	-1	***1***
1	-1	-1	-1	-1	***1***
1	-1	-1	1	1	***1***
1	-1	1	-1	1	***1***
1	-1	1	1	-1	***1***
1	1	-1	-1	1	***1***
1	1	-1	1	-1	***1***
1	1	1	-1	-1	***1***
1	1	1	1	1	***1***

TABLE 3.—CONDITIONS FOR THE 16 CASES OF TABLE 2 THAT WERE SELECTED FOR TESTING OUT OF 32 POSSIBLE CASES (TABLE 1). DUPLICATE FATIGUE TESTS WERE PERFORMED IN A TOTAL OF 32 FATIGUE TESTS

Coating Thickness - μm	Shot Peening - 4N-100% or 16N-200%	log (pO_2- MPa)	760C Oxidation -h	760C Corrosion -h
0	4N-100%	-15.8	0	50
0	4N-100%	-15.8	500	0
0	4N-100%	-1.7	0	0
0	4N-100%	-1.7	500	50
0	16N-200%	-15.8	0	0
0	16N-200%	-15.8	500	50
0	16N-200%	-1.7	0	50
0	16N-200%	-1.7	500	0
26.5	4N-100%	-15.8	0	0
26.5	4N-100%	-15.8	500	50
26.5	4N-100%	-1.7	0	50
26.5	4N-100%	-1.7	500	0
26.5	16N-200%	-15.8	0	50
26.5	16N-200%	-15.8	500	0
26.5	16N-200%	-1.7	0	0
26.5	16N-200%	-1.7	500	50

Results and Discussion

Specimen Surface Conditions

The effects of specimen preparation steps on surface conditions are compared in Figures 3(a) to (c) for uncoated bars and Figures 3(d) and (f) coated bars after (a) initial machining, (b) machined plus shot peening 4 N-100% plus specimen preparation treatment, (c) machined plus shot peening 16 N-200% plus specimen preparation treatment, (d) as-coated, (e) coating plus shot peening 4 N-100% plus specimen preparation treatment, and (f) coating plus shot peening 16 N-200% plus specimen preparation treatment. Figure 3(d) shows large spherical features on the surface (yellow arrow) referred to as spits which occur during coating due to occasional arcing events in the plasma. Larger spits are believed to flatten during shot peening and create some of the larger folds or laps in the surface, as indicated by the yellow arrows in Figure 3(e). In addition, grit blasting has been observed to create large depressions in the surface which also results in the formation of "pushed up" metal into elevated mounds. These mounds also flatten during shot peening and form folds and laps on the surface, as indicated by the red arrow in Figure 3(c). Corresponding average roughness is shown in Figure 4. Machining of the fatigue test specimens by low stress grinding and longitudinal polishing (LP) in the axial direction produced very fine polishing grooves in the axial direction (Fig. 3(a)) with an average roughness of only ~0.1 μm (Fig. 4). Grit blasting and coating this surface eliminated the axial grooved texture producing a nondirectional nodular coating texture (Fig. 3(d)) that increased the measured roughness over that of the as-machined+LP surface (Fig. 4). Shot peening of both the uncoated and coated bars eliminated earlier features, with the formerly grooved and nodular surface textures mostly eliminated, being replaced with an undulating, dimpled

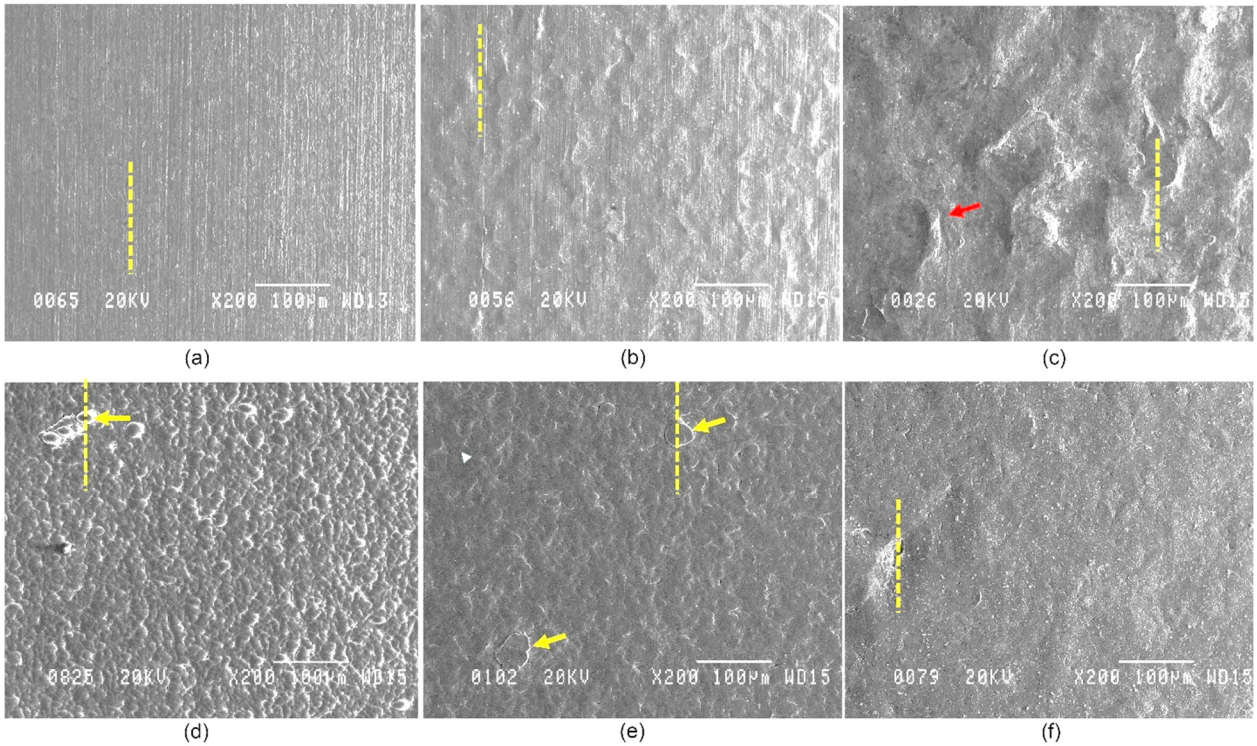

Figure 3.—Fatigue specimen surfaces: (a) as-machined, (b) machined, shot peened 4N-100%, preparation treated, (c) machined, shot peened 16N-200%, preparation treated with the red arrow indicating a lap (see text) (d) as-coated with the yellow arrow indicating a series of spits (see text), (e) coated, shot peened 4N-100%, preparation treated, (f) coated, shot peened 16N-200%, preparation treated. Yellow dashed lines indicate prominent features which were scanned (see text). The longitudinal polishing (LP) and specimen loading axes are both oriented vertically.

texture (Figs. 3(b), (c), (e), and (f)). Shot peening of the coated surface resulted in folds of metal ("laps") sometimes occurring at the edges of dimples created by the impact of shot (Fig. 3). This shot peened texture was finer in scale for coated specimens than for uncoated specimens (compare Figs. 3(b), (e), (c), and (f)). Uncoated specimens with 16 N-200% shot peening had highest average roughness.

Surface profiles of features noted in Figure 3 are shown in Figure 5. Prominent coating nodules ("spits") were observed to be scattered on the surfaces for all coated test specimens (Fig. 3(d)). These spits are believed to be ejected from the target during random arcing events in the plasma. The prominent coating spits were largely suppressed by shot peening. The dimples produced by shot peening in both uncoated and coated specimens had modest depths. However, more widely scattered deeper depressions were observed in coated specimens, which remained after shot peening. These coated depressions were determined to be formed by grit blasting of specimens before their coating, and deeper depressions sometimes remained prominent after coating and shot peening.

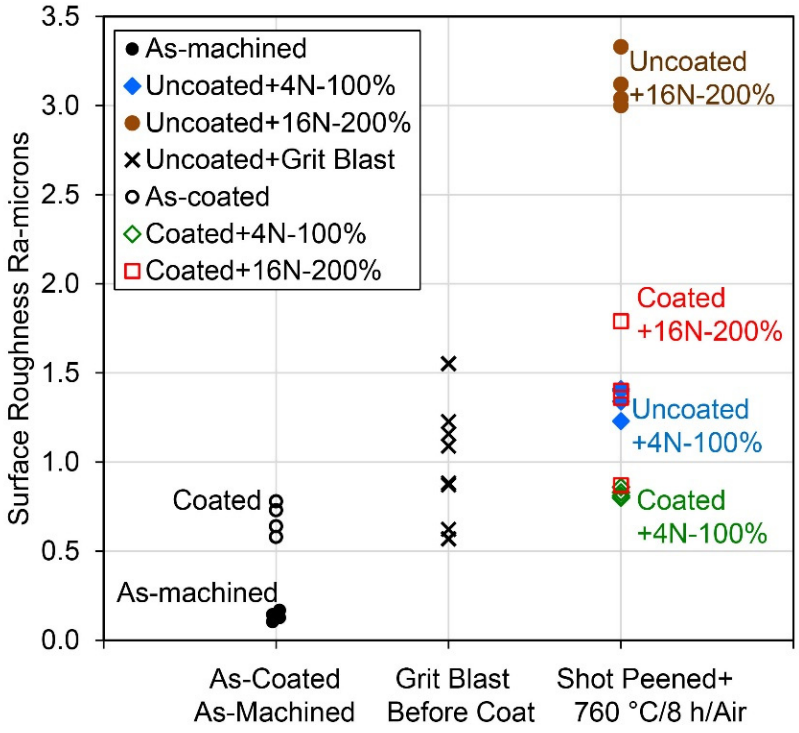

Figure 4.—Average surface roughness Ra for the cases shown in Figure 3 as-machined, as-coated and after shot peening and preparation treatment (760 °C for 8 h in air).

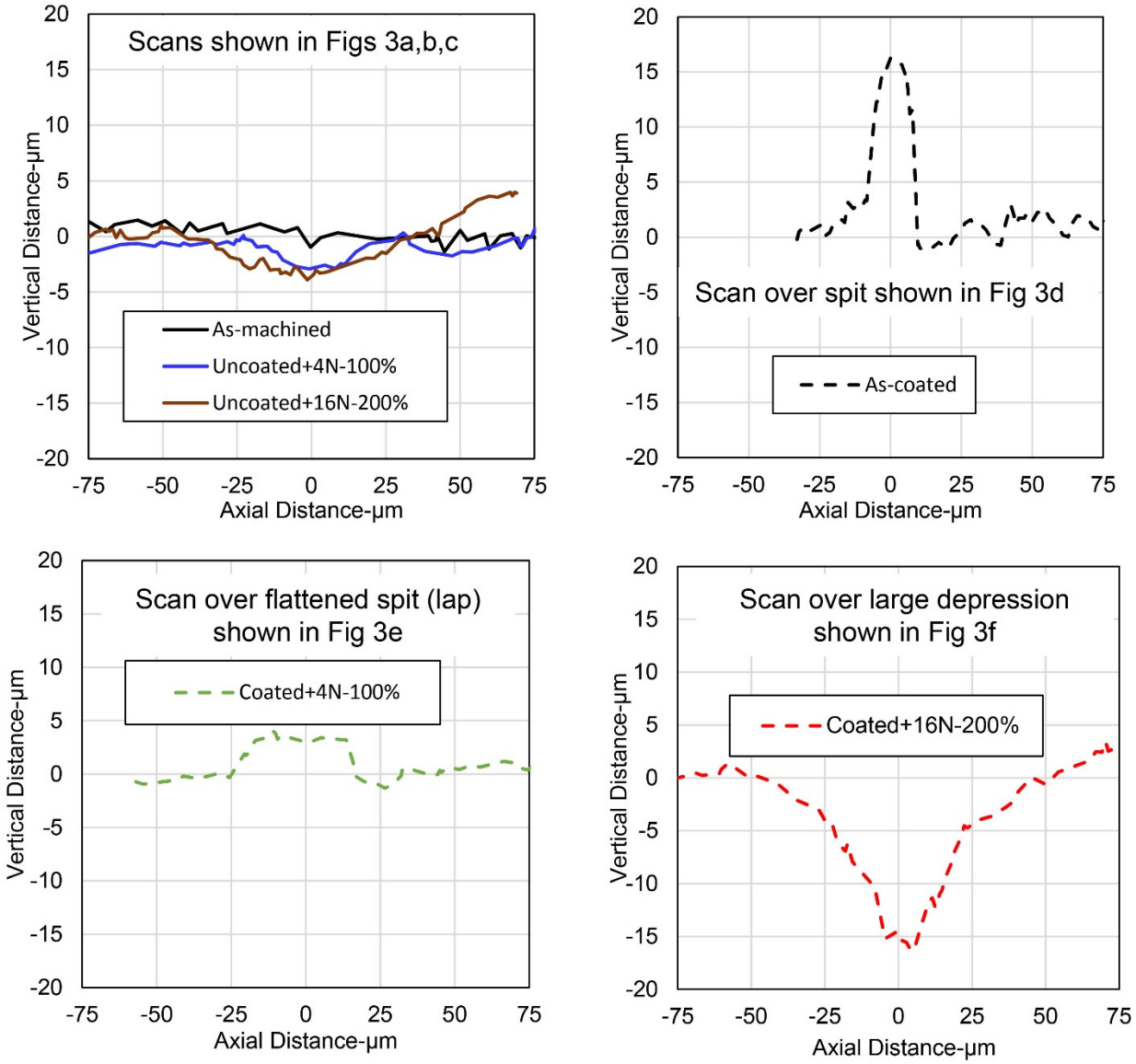

Figure 5.—Surface profile measurements of selected prominent features for each case shown in Figure 3 (see yellow dashed lines). Measurements were made parallel to the specimen loading axis.

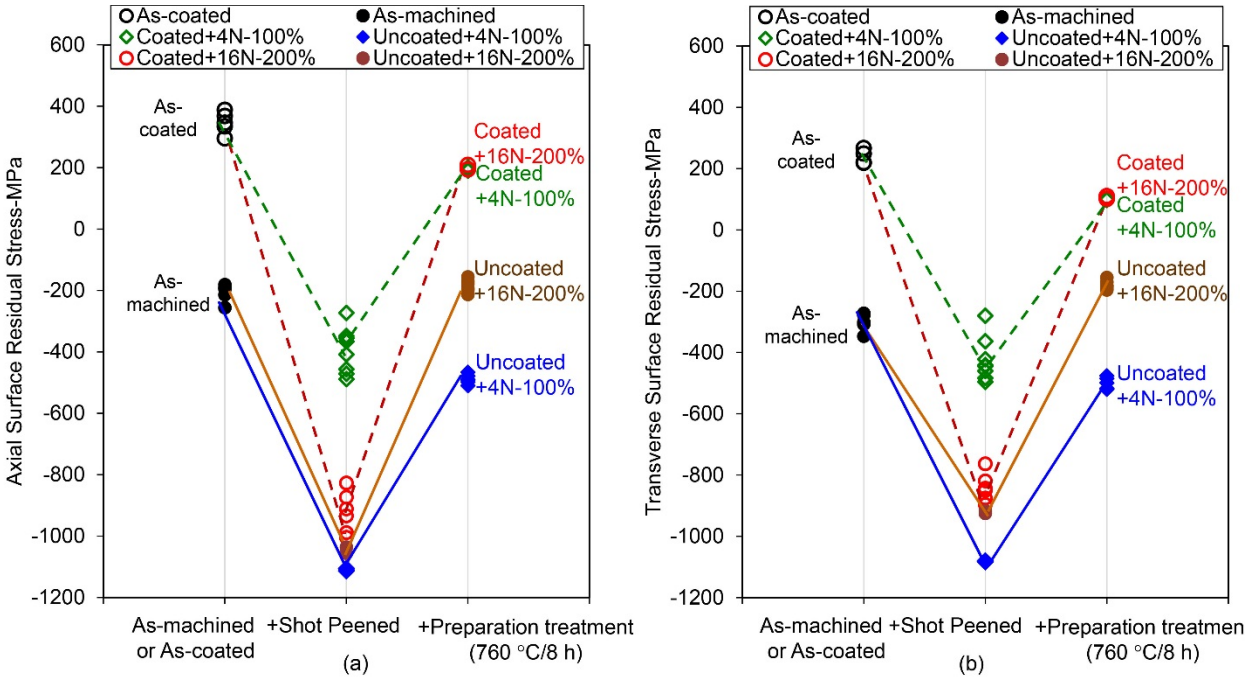

Figure 6.—Residual stresses measured on the surfaces: (a) axial residual stress measured parallel to the specimen loading axis, (b) transverse residual stress. While shot peening produced beneficial compressive residual stresses at the surface for uncoated and coated specimens, subsequent preparation treatment at 760 °C for 8 h (regardless of low or high pO_2) relaxed out much of these stresses, especially for coated specimens. Filled symbols indicate uncoated specimen surfaces, hollow symbols indicate coated specimen surfaces.

The residual stresses measured at the surface also varied as a function of processing steps, as compared in Figure 6. Machining of the fatigue test specimens produced approximately –200 and –300 MPa compressive residual stresses at the surface in the axial and transverse directions, respectively. These compressive stresses remained after grit blasting. However, coating of this surface drastically changed the residual stresses, producing modest tensile surface residual stresses (350 to 230 MPa) in the coating for the axial and transverse directions. Yet, varied coating application processes can themselves introduce varied residual stresses in coatings of similar composition. For example, compressive residual stresses near –500 MPa were reported in Ni-20Cr and Ni-50Cr coatings applied by cold spraying onto steel (Ref. 23). However, the present coating process utilized physical vapor deposition, which did not have the high speed impacts of solid powder particles such as in cold spraying. Subsequent shot peening at 16 N-200% produced comparable compressive residual stresses for both uncoated and coated surfaces. However, shot peening at 4 N-100% produced distinctly lower magnitudes of compressive residual stress for the coated surface. The reasons for this lower stress response of the coating at this low shot peening condition are not clear, but could be related to the effects of lower strength and hardening of the coating than that of the substrate (Ref. 22). High intensity shot peening has been shown to produce a “hook” near the surface for superalloys, where the magnitude of induced compressive residual stress is lower at the surface than beneath the surface due to high plasticity (Ref. 14). Such an effect could be encouraged by the coating’s lower mechanical properties.

Final specimen preparation treatment at 760 °C for 8 h at low or high pO_2 relaxed compressive surface residual stresses for both uncoated and coated surfaces, Figure 6. After shot peening and preparation treatment, the uncoated specimens had only modest compressive residual stresses measured at the surface of approximately –575 MPa for 4 N-100% shot peening and –200 MPa for 16 N-200% shot peening. This is consistent with past work showing that higher shot peening coverage usually induces higher plasticity near the surface of a given superalloy (Ref. 17). This higher plasticity can enhance the relaxation of residual stresses during thermal exposures, related to dislocation recovery.

Preparation-treated coated specimens had modest tensile residual stresses of near +200 MPa at the surface for both shot peening conditions. Subsequent evaluations of residual stress beneath the surface and the effects of fatigue cycling on these stresses indicated that significant compressive residual stresses of over –400 MPa remained at depths up to 150 μm for both coated and uncoated specimens (Ref. 22).

The generation of compressive residual stresses in the coating by shot peening has been described for MCrAlY coatings applied by various processes (Ref. 24) and for NiCr coatings on superalloys (Ref. 23). However, the complete relaxation in the coating of these compressive stresses during the subsequent preparation treatment at the high temperature used in the present study was not reported or expected. This response of the coating appears to be related to the low strength and stress relaxation resistance of such coatings (Ref. 22).

Fatigue Lives

Fatigue lives are compared in Figure 7 for all specimens tested. Figures 7(a) and (b) show life versus partial pressure of oxygen of the specimen preparation treatment, in order to clearly inspect fatigue lives for each separate case after no exposures, and after oxidation plus hot corrosion exposures. It was apparent that without exposures, uncoated specimens with 4 N-100% shot peening had superior average life for the processing combinations tested, as shown in Figure 7(a). However, with corrosion or the combination of both oxidation and corrosion, uncoated specimens with this low shot peening had large

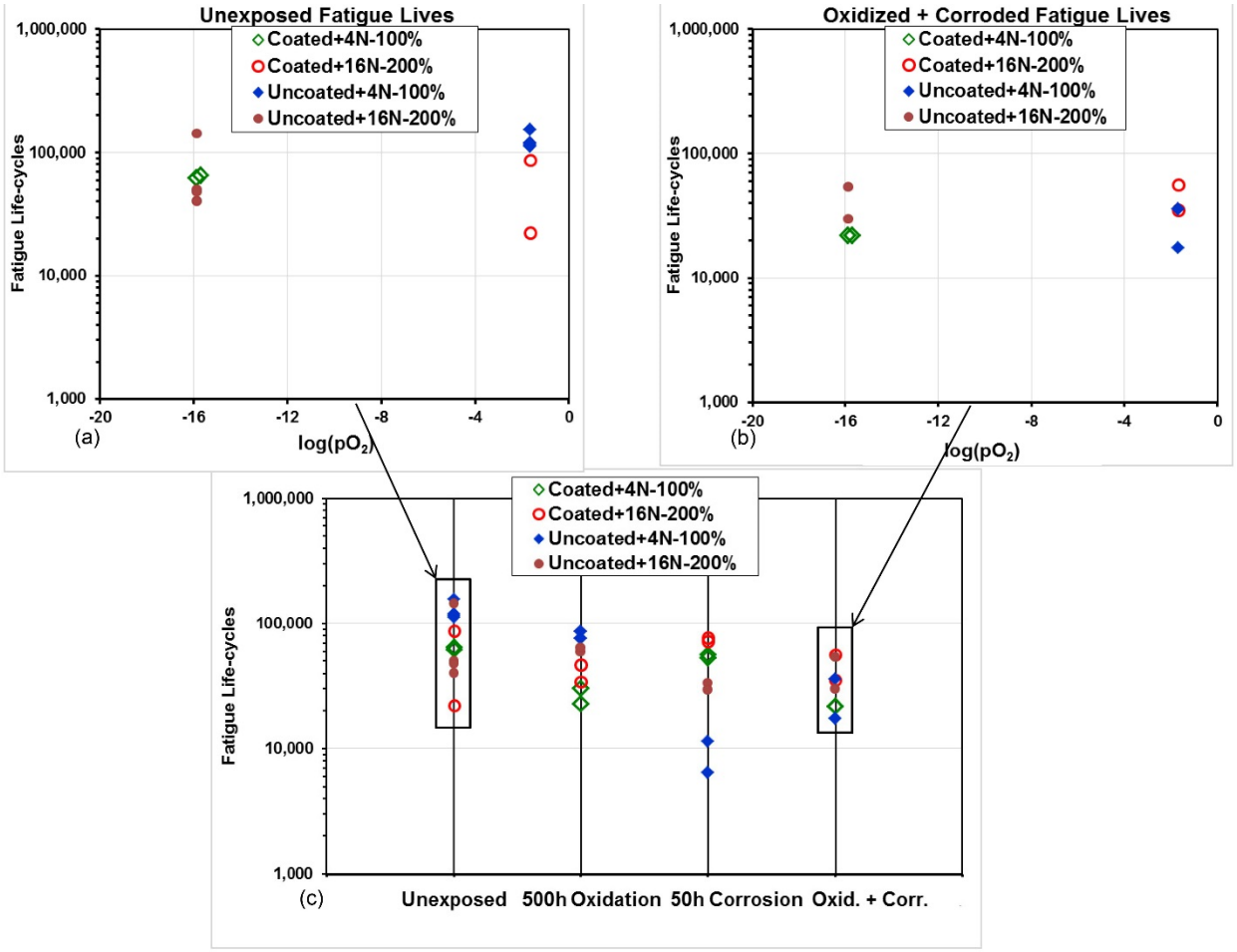

Figure 7.—Comparisons of fatigue life for all cases tested: (a) with no exposures, (b) with oxidation plus corrosion exposures, (c) all cases tested. Filled symbols indicate uncoated specimens, hollow symbols indicate coated specimens.

reductions in fatigue life, Figures 7(b) and (c), especially for the case of 50 h hot corrosion exposure, Figure 7(c). Yet, for other processing combinations that included a coating, these exposures could be sustained with only minor reductions in life. Due to the nature of this experimental design, statistical analysis was necessary to more fully evaluate the effects of each variable.

Step-wise forward and reverse selections of potential terms were performed using least square linear regression, with only terms each having an effect with statistical significance of at least 95% selected for inclusion in the resulting linear regression equation. Some variables were found to have a consistent significant influence on fatigue life, and hence contributed a linear term to the equation. Other variables had a significant influence on life that varied with the level of another variable, and hence contributed an associated paired product term to the equation. The same regression equation resulted using both forward and reverse step-wise selections of terms from among the normalized variables hot corrosion (***HC'***), oxidation (***O'***), shot peening (***SP'***), coating thickness (***C'***), common logarithm of partial pressure of oxygen during heat treatment (***LP'***), and their paired products:

$$\text{Log}(N_f)=4.6320-0.1534*\boldsymbol{HC'}-0.0683*\boldsymbol{O'}+0.0492*\boldsymbol{SP'}+0.1195*\boldsymbol{C'}*\boldsymbol{HC'}-0.1129*\boldsymbol{C'}*\boldsymbol{O'}-0.0454*\boldsymbol{C'}*\boldsymbol{LP'}$$
$$+0.0769*\boldsymbol{SP'}*\boldsymbol{HC'}-0.0617*\boldsymbol{SP'}*\boldsymbol{LP'}-0.0746*\boldsymbol{LP'}*\boldsymbol{O'}$$
$$R^2_{adj} = 0.81, \text{ rms Error} = 0.1309$$

This equation had a satisfactory coefficient of determination after adjustment for the number of terms, with $R^2_{adj} = 0.81$. The root mean square error between actual and modeled log life was 0.1309. For an estimated life of 10,000 cycles, this root mean square error was ±3,518 cycles. For an estimated life of 100,000 cycles, this root mean square error was ±35,176 cycles. This agreement is depicted in the plot of actual values for fatigue life versus the model's estimates in Figure 8.

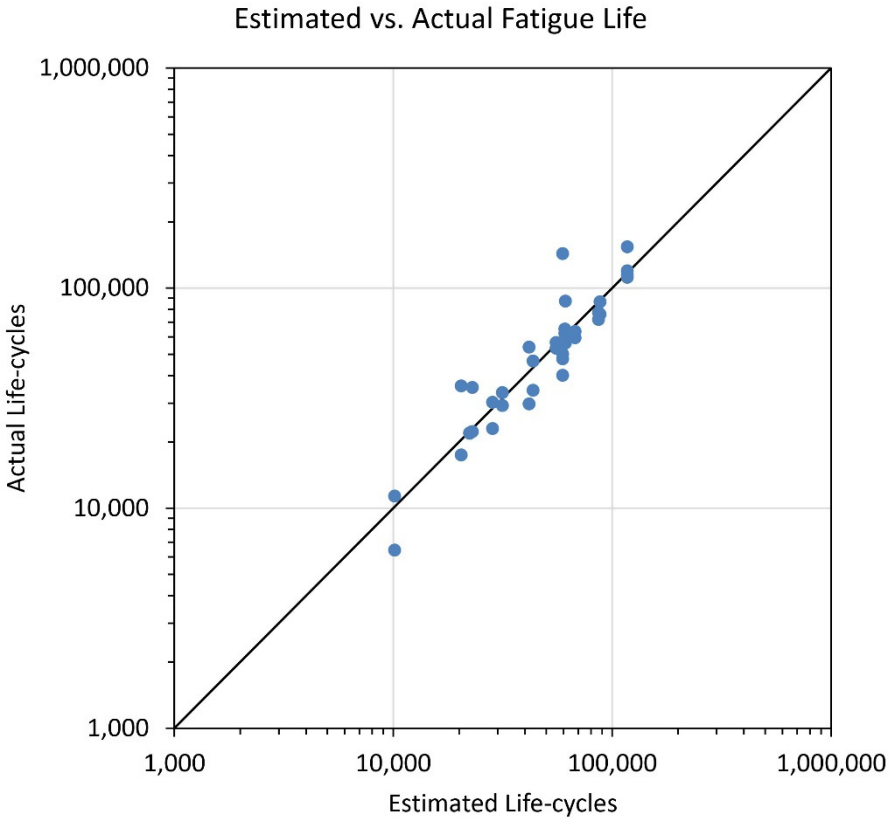

Figure 8.—The regression model's estimates versus actual values of fatigue life.

The derived regression equation included many terms, indicating many significant factors influenced the fatigue lives measured. The equation indicated that hot corrosion time had the strongest linear effect on fatigue life, followed by oxidation time, with both effects reducing life. Shot peening had a smaller linear effect, increasing fatigue life. Three paired-product (interaction) terms involving the coating were also significant, indicating the coating had a strong influence on several other variables. Two of these terms dealt with exposures, indicating hot corrosion exposures were less harmful for coated specimens, but that oxidation exposure was more harmful for coated specimens. These conflicting interactions of the coating with exposures were unexpected. It may be that the long oxidation time of 500 h at 760 °C allowed time for inter-diffusion as well as oxidation to affect coating composition and phase contents as functions of depth from the surface, which could influence fatigue resistance. This will be revisited in a later section. Two interaction terms involving shot peening were significant, showing shot peening was also influential on other variables. They indicated that hot corrosion exposures were less harmful to fatigue life for high shot peening, and that shot peening was more beneficial to fatigue life when followed by specimen preparation treatment at a low partial pressure of oxygen. The two remaining interaction terms indicated that specimen preparation treatment at a low partial pressure of oxygen helped reduce the effects of subsequent oxidation on fatigue life, and that the low partial pressure of oxygen during the preparation treatment improved the life of coated specimens. This may reflect that preparation treatment at the low partial pressure of oxygen produced a more protective, Cr_2O_3 – rich oxide scale on both uncoated and coated specimens, as previously reported for bulk Co30Cr (Ref. 26).

This screening test matrix and resulting linear regression model had been intended to screen the linear effects of these five variables and their pair-wise interactions. Additional test cases would be necessary to assess the linearity of each variable, and to generate a response surface model that could best optimize response. Nevertheless, the regression model could be used to inspect the effects of variables, and to project the settings of variables which would give higher fatigue life for different exposures. For high fatigue life without exposures, the model indicated no coating combined with low shot peening and specimen preparation treatment in air were preferred. The higher magnitude of compressive residual stress measured at the surface for the case of 4 N-100% plus preparation treatment in air (Fig. 6) could be dominant in maximizing life here, while the actual effect of differences in oxide layers produced by the preparation treatment in air or low pO_2 may be less important. For high fatigue life after both full oxidation and full hot corrosion exposures, the coating combined with high shot peening and preparation treatment at low partial pressure of oxygen were deemed more favorable. Though this combination of conditions had not been included in the test matrix, it has subsequently been confirmed to indeed give higher fatigue life after these exposures. These same conditions were also necessary for high fatigue life after only the full hot corrosion exposure. Now this combination of conditions had been included in the test matrix, and it did give relatively high fatigue life. So overall, the coating did help mitigate the reductions in fatigue life due to these exposures.

Failure Initiation Sites

Typical fractures surfaces of specimens not subjected to oxidation or hot corrosion exposures are shown in Figures 9 and 10. Uncoated specimens without exposures often failed from nonmetallic inclusions within the interior of the gage section, as shown in Figure 9(a). These were usually granulated Type II (Ref. 27) aluminum oxide inclusions that were 43 μm to 137 μm wide, and 14 μm to 44 μm thick. Only a very few surface cracks under 100 μm in width were observed on the gage surface adjacent to the failure initiation site, as shown in Figure 10(a). Coated specimens without exposures most often failed from coated depressions on the surface, as shown in Figure 9(b). These depressions, which had been noted in Figures 3 and 5, had been formed during grit blasting before application of the coating. Examinations of all coated specimens indicated the coated depressions causing failure were 120 μm to 138 μm wide, and 16 μm to 42 μm deep. Many surface cracks 17 μm to 1,225 μm in width along the surface were observed on the coated gage surface adjacent to the failure initiation site, as shown in Figure 10(b). At this location, cracks on the surface are unloaded during crack growth at the failure

initiation site, and are not expected to widen due to enhanced stresses of the specimens' remaining load bearing cross section. Only about 5% of these cracks were typically initiated from a noticeable depression. This indicated that the coating had enhanced cracking, which was independent of the presence of depressions. Cracks opposite this location on the specimen were observed to significantly widen due to plastic deformation of the sample during the remote crack growth at the failure initiation site, as well as at specimen failure. Hence, these cracks were not included in the presented images or measurements.

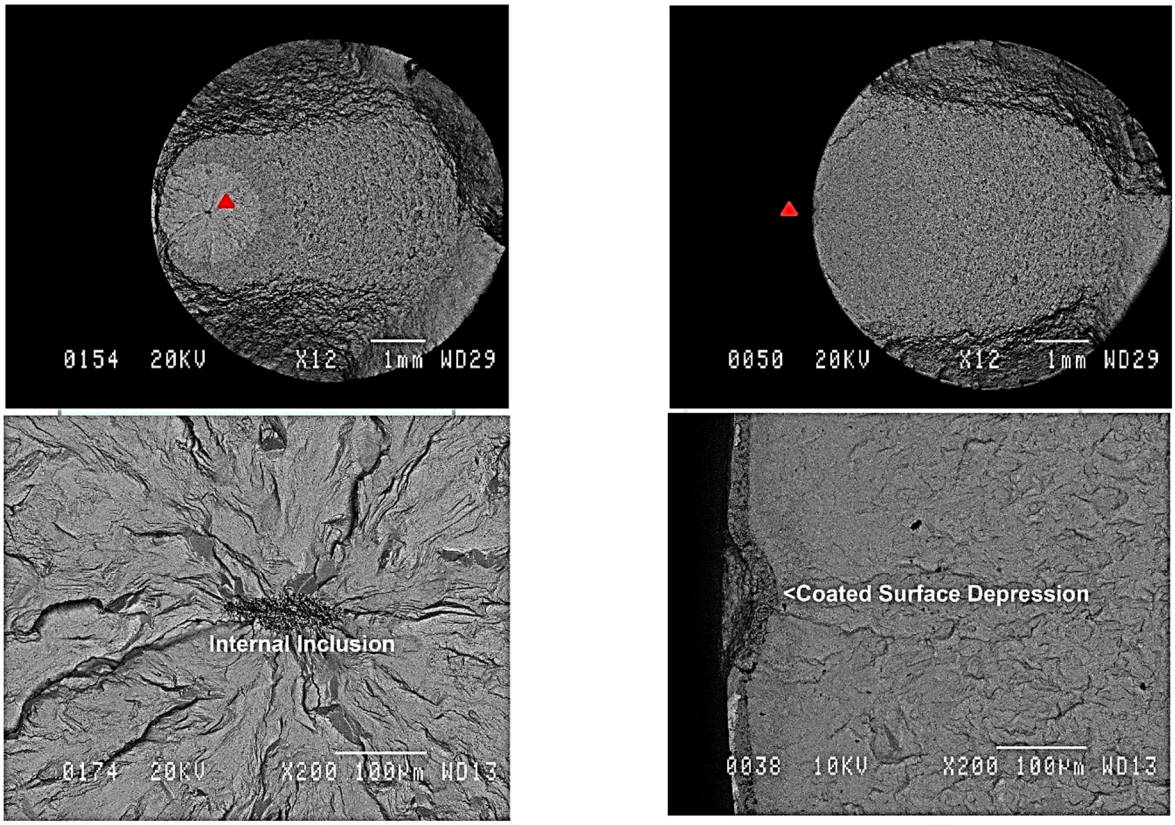

Figure 9.—Typical fracture surface—failure initiation point (red triangle) for unexposed fatigue specimens: (a) uncoated—internal inclusion, and (b) coated—coated surface depression.

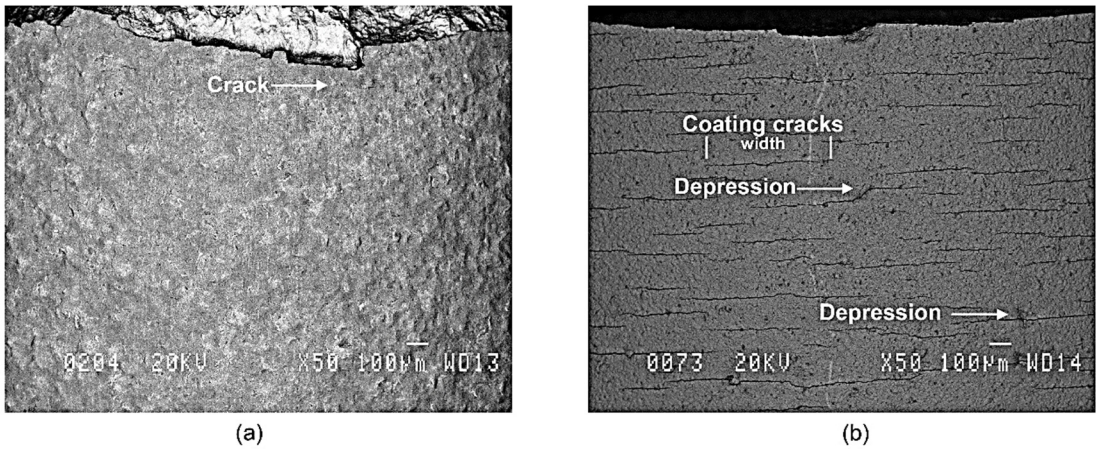

Figure 10.—Typical side of the fracture surface, adjacent to the failure initiation point, for unexposed specimens: (a) uncoated, (b) coated. More fatigue cracks formed at the coating surface than for uncoated specimens. The specimen loading axis is oriented vertically.

Typical fractures surfaces of specimens subjected to oxidation and hot corrosion exposures are shown in Figures 11 and 12. Uncoated specimens with the oxidation-only exposure had multiple fatigue cracks initiating at the outer surface oxide layer to cause failure, as shown in Figures 11(a) and 12(a). Uncoated specimens with the hot corrosion-only exposure and those having both the oxidation and hot corrosion exposure failed from numerous corrosion pits that were up to 394 μm wide and up to 63 μm deep, as shown in Figures 11(b) and 12(b). Coated specimens having either or both oxidation and hot corrosion exposures still had failures initiating from the coated depressions, as shown in Figure 11(c) but showed no corrosion pit formation. Yet, examination of the coated gage surface adjacent to the main failure initiation site again disclosed many other fatigue cracks on the oxidized coating surface. Therefore, the oxidized/ corroded coating surface again had enhanced fatigue cracking but without obvious corrosion pits.

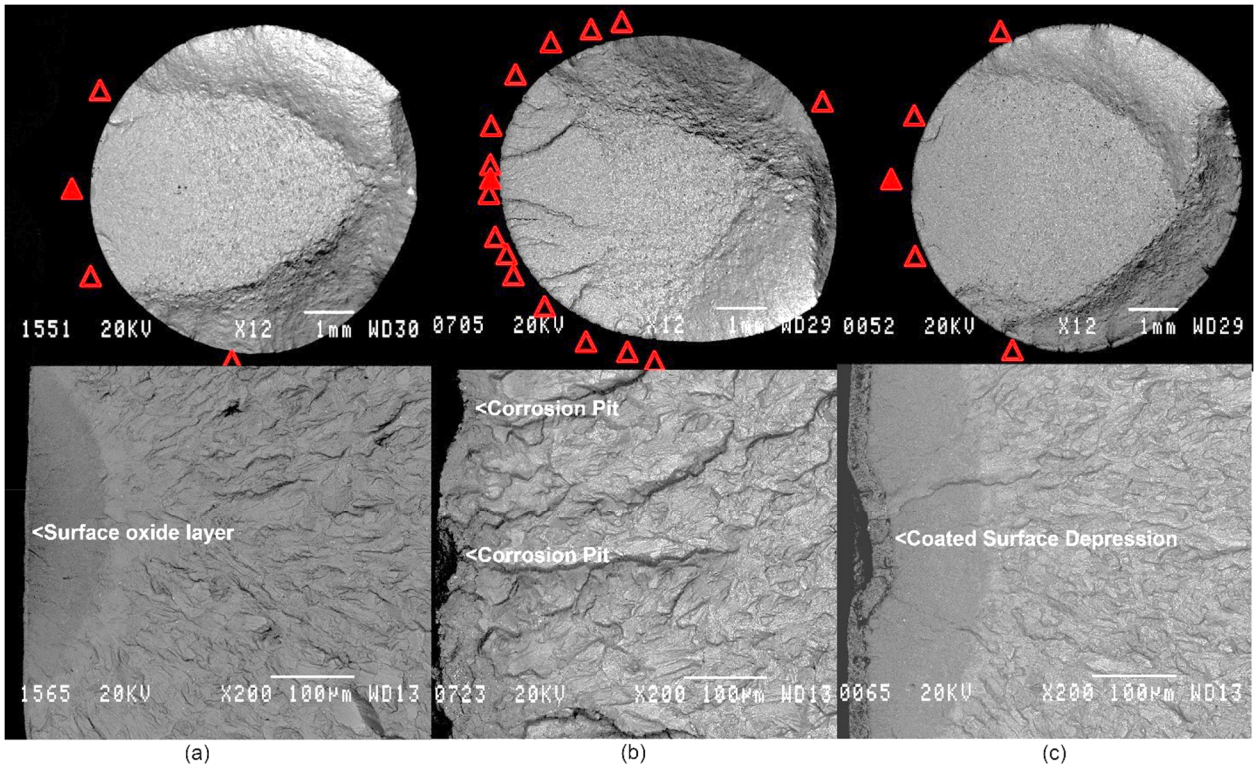

Figure 11.—Typical fracture surface - failure initiation points for exposed fatigue specimens: (a) uncoated, oxidized 500 h at 760 °C, (b) uncoated, hot corroded 50 h at 760 °C, and (c) coated, oxidized and hot corroded at 760 °C. Uncoated specimens after exposures had surface-initiated failures from surface oxides and corrosion pits, while the coating prevented pits from exposing the superalloy and initiating fatigue cracks.

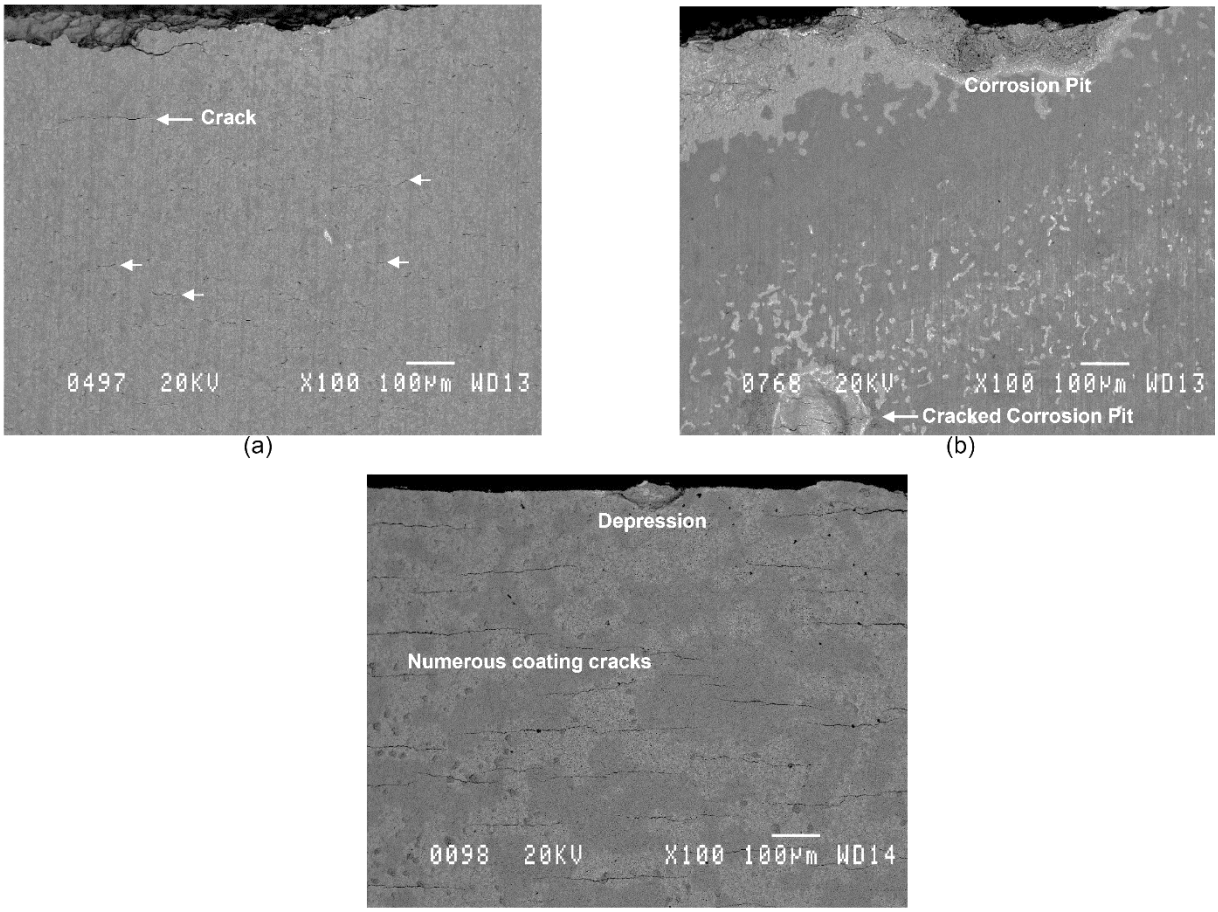

Figure 12.—Typical side of the fracture surface, adjacent to the failure initiation point, for exposed specimens: (a) uncoated, oxidized 500 h, (b) uncoated, hot corroded 50 h, (c) coated, oxidized and corroded. More numerous fatigue cracks formed at the coating surface than for uncoated specimens. The specimen loading axis is oriented vertically.

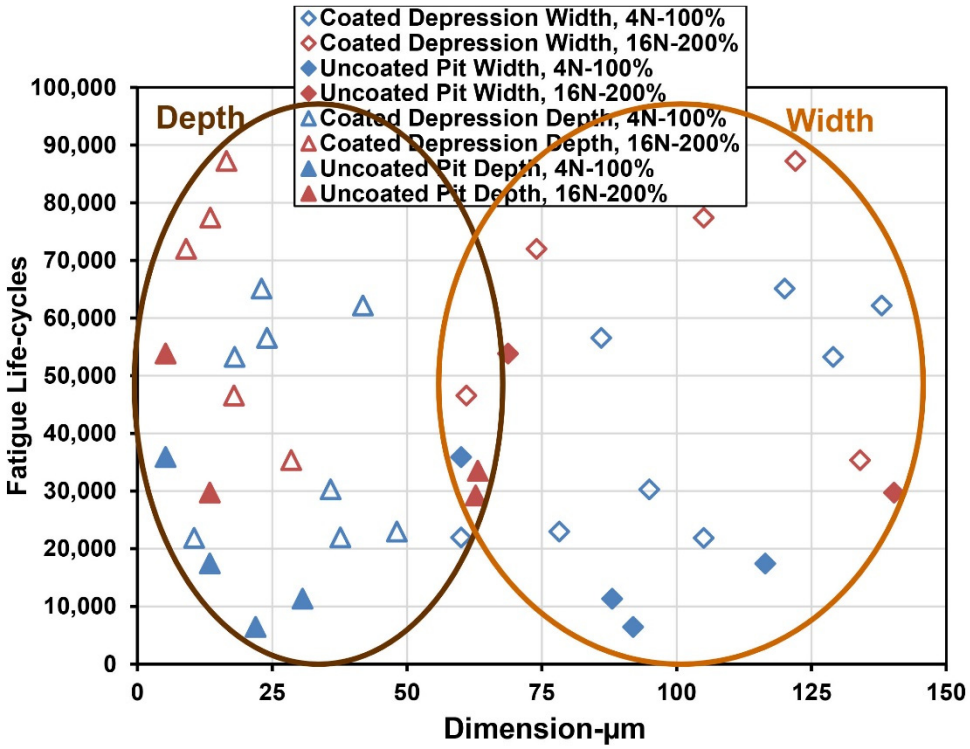

Figure 13.—Comparison of two life limiting defects—Coating depressions and corrosion pits. The corrosion pits (filled symbols = pit in legend) that initiated failures in machined specimens had similar dimensions but gave lower fatigue lives than the depressions (hollow symbols) present on coated specimens.

It was interesting to compare the dimensions of these life-limiting surface defects: coated depressions versus hot corrosion pits. A simple comparison is presented in Figure 13. The corrosion pits (filled symbols) that initiated failures in uncoated specimens had similar dimensions but gave lower fatigue lives than the depressions (hollow symbols) present on coated specimens. This could be attributed in part to the effects of adjacent corrosion pits giving more highly concentrated stresses at their junctions and hence being earlier crack initiation sites (Ref. 11), in comparison to the larger, but more widely scattered depressions. This could also indicate that the corrosion-formed oxide layers formed at pits in the superalloy (Ref. 27) are more prone to pre-mature cracking than the coating or superalloy substrate, even when the pits are more widely separated. Investigations of the latter aspect would require interrupted tests.

Polished cross-sections are shown in Figures 14(a) and (b) from uncoated and Figures 14(c) and (d) from coated specimens that were subjected to oxidation exposure in air for 500 h at 760 °C and the hot corrosion test as above, followed by fatigue cycling to failure at 760 °C. The polishing plane for these test specimens was parallel to the loading direction. The plane sectioned the largest fatigue crack causing failure in each specimen. Therefore, the cracks in each image were unloaded as the main crack grew, and not overloaded. Oxidized cracks can be seen growing along grain boundaries from the surface of the uncoated specimen. A polished cross-section is shown for comparison in Figures 14(c) and (d) for a coated specimen that was subjected to the same oxidation exposure in air for 500 h at 760 °C and the hot corrosion test, followed by fatigue cycling to failure at 760 °C. The polishing plane for the coated test specimen in Figures 14(c) and (d) was again parallel to the loading direction. Cracks can be seen penetrating the coating but show minimal extension into the substrate. Only the mid portion of the coating still contains the initial content of high-Cr alpha phase. It appears that the long oxidation time of 500 h at 760 °C allowed time for outer oxidation as well as interdiffusion with the substrate to affect coating phases. Some high-Cr alpha phase particles were apparently dissolved near the outer surface, to support

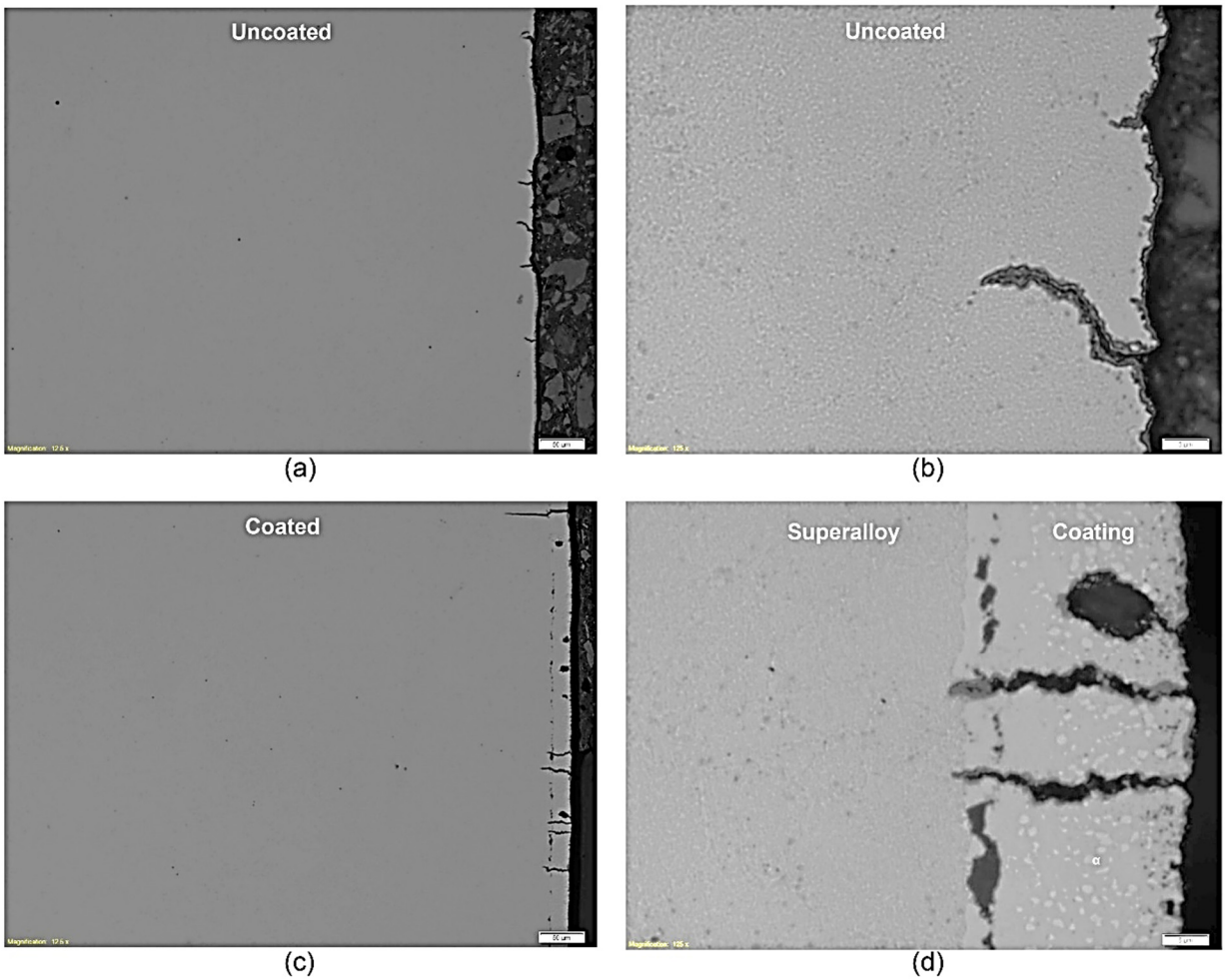

Figure 14.—Metallographic sections prepared from fatigue specimens that had been oxidized 500 h and hot corroded 50 h at 760 °C, then fatigue tested to failure at 760 °C: (a) and (b) uncoated, (c) and (d) coated. The polishing plane was prepared parallel to the loading direction (oriented vertical in the images), and sectioned the largest fatigue crack causing failure in each specimen. Therefore, the cracks in each image were unloaded as the main crack grew, and not overloaded. Many cracks were initiated in the coating, which often did not continue growing deep into the superalloy substrate. Light shaded particles in coating are α-Cr.

formation of the chrome-oxide layer. Also, alpha phase was absent adjacent to the superalloy. Here, inter-diffusion with the substrate, likely during the 500 h oxidation exposure, has resulted in recession of the alpha phase. Each of these aspects could influence fatigue resistance. This may help to explain the interaction term in the derived regression equation, which indicated that long oxidation exposure time was more harmful to fatigue life of coated specimens. Indeed, multiple secondary fatigue cracks appeared to grow through the coating, yet many still did not extend into the underlying superalloy. The apparent thickness of the surface-connected oxide-filled cracks sometimes was widened within the coating. These appeared to be sometimes due to the crack plane twisting to near that of the metallographic polishing plane. In other cases it appeared that surface-connected coating defects may have been attacked at an accelerated rate (Figs. 14(c) and (d)), a subject of further investigation. Nevertheless, no corrosion pits were found that penetrated completely through the coating to attack the superalloy substrate during the corrosion treatment. Therefore, the coating did appear to be robust enough to protect the substrate superalloy from corrosion attack and pit formation for the present conditions in the presence of these changes from extended oxidation exposures, while preserving fatigue life when favorably shot peened and heat treated.

Further improvements in coated fatigue life could be possible, even with such oxidation and hot corrosion exposures. Refinements could be evaluated for the surface treatment before coating, the coating application process, post-coating shot peening, and the final preparation treatment.

Summary of Results

LSHR fatigue test specimens were coated with a NiCrY coating, and then shot peened and preparation treated at purposefully varied conditions along with uncoated test specimens. Bumps or "spits" were produced on the coating surface, which shot peening could largely suppress. However, scattered coated depressions in the surface, which were produced during grit blasting before coating, still remained. Shot peening also produced beneficial compressive residual stresses in the coating, yet these stresses were eliminated during the subsequent preparation treatment. Coated and uncoated specimens were oxidized, corroded, or both at 760 °C, then fatigue tested to failure at this temperature. For comparison, coated and uncoated specimens were also fatigue tested without the hot corrosion or oxidation exposures. Hot corrosion for 50 h had a stronger effect than oxidation for 500 h, but both significantly reduced subsequent fatigue life. The regression model indicated the reduction in life could be minimized by using the coating with 16N-200% (high) shot peening followed by a specimen preparation treatment of 760 °C for 8 h in a low partial pressure of oxygen. Failure evaluations indicated the coating did not allow distinct corrosion pits to form, penetrate to the underlying superalloy, and initiate earlier fatigue cracks and failures, as observed in uncoated specimens. Yet, the coating had enhanced fatigue cracking, including from the scattered coated depressions. Examinations of metallographically prepared longitudinal sections of the coated specimens with and without exposures before fatigue testing indicated the secondary coating cracks observed on the gage sides often did not grow into the superalloy substrate.

Conclusions

1. Shot peening can make the surface of this coating more uniform; however, the generated compressive residual stresses are not maintained in the coating at high temperatures.
2. Hot corrosion and oxidation exposures at 760 °C can significantly reduce fatigue life:
   a. Uncoated specimens—Corrosion pits and oxidation layers can initiate fatigue cracks to reduce life for the examined test conditions.
   b. Coated specimens—The coating can prevent corrosion pits from forming. Yet, cracks can form sooner in the coating during fatigue cycling, including at defects such as depressions formed during grit blasting before coating.
3. To maximize fatigue resistance after such oxidation and corrosion exposures, application of this type of coating, followed by shot peening near 16 N-200% and a specimen preparation treatment near 760 °C for 8 h in a low partial pressure of oxygen should be considered. Alternative surface pre-treatments before coating should also be screened.

References

1. R. Schafrik, R. Sprague, "Superalloy Technology–A Perspective on Critical Innovations for Turbine Engines," Key Engineering Materials, V 380, 2008, pp. 113–134.
2. M.R. Bache, J.P. Jones, G.L. Drew, M.C. Hardy, N. Fox, "Environment and Time Dependent Effects on the Fatigue Response of an Advanced Nickel Based Superalloy," Int. J. Fat., V 31 (11–12), 2009, pp. 1719–1723.

3. A. Encinas-Oropesa, G. Drew, M. Hardy, A. Leggett, J. Nicholls, and N. Simms, "Effects of Oxidation and Hot Corrosion in a Nickel Disc Alloy," Superalloys 2008, ed. R.C. Reed, K.A. Green, P. Caron, T.P. Gabb, M.A. Fahrmann, E.S. Huron, S.A. Woodard, The Mining, Metallurgy, and Materials Society, Warrendale, PA, 2008, pp. 609–618.
4. C.K. Sudbrack, S.L. Draper, T. Gorman, J. Telesman, T.P. Gabb, D.R. Hull, "Oxidation and the Effects of High Temperature Exposures on Notched Fatigue Life of an Advanced Powder Metallurgy Disk Superalloy," Superalloys 2012, E.S. Huron, R.C. Reed, M.C. Hardy, M.J. Mills, R.E. Montero, P.D. Portella and J. Telesman, Eds., TMS, Warrendale, PA, 2012, pp. 863–872.
5. R.A. Rapp, "Hot Corrosion of Materials: A Fluxing Mechanism?", Corros. Sci., 2002, 44, pp. 209–221.
6. F.S. Pettit and C.S. Giggins, "Hot Corrosion," Superalloys II, C.T. Sims, N.S. Stoloff, and W.C. Hagel, Eds., John Wiley & Sons, New York, 1987, pp. 327–358.
7. B. Gleason, "High-Temperature Corrosion of Metallic Alloys and Coatings," Materials Science and Technology, ed. R.W. Cahn, P. Haasen, E.J. Kramer, John Wiley & Sons Inc., 2000, pp. 173–228.
8. J.R. Groh and R.W. Duvelius, "Influence of Corrosion Pitting on Alloy 718 Fatigue Capability," Superalloy 718, 625, 706 and Derivatives, ed. E.A. Loria, The Mining, Metallurgy, and Materials Society, Warrendale, PA, 2001, pp. 583–592.
9. G.S. Mahobia, N. Paulose, S.L. Mannan, R.G. Sudhakar, K. Chattopadhyay, N.C.S. Srinivas, "Effects of Hot Corrosion on the Low Cycle Fatigue Behavior of IN718," Int. J. Fat., V. 59, 2014, pp. 272–281.
10. J.K. Sahu, R.K. Gupta, J. Swaminathan, N. Paulose, S.L. Mannan, "Influence of Hot Corrosion on the Low Cycle Fatigue Behavior of SU 263," Int. J. Fat., V. 51, 2013, pp. 68–73.
11. J. Telesman, T.P. Gabb, Y. Yamada, S.L. Draper, "Fatigue Resistance of a Hot Corrosion Exposed Disk Superalloy at Varied Test Temperatures," Mat. at High Temperatures, V. 33 (4-5), 2016, pp. 517–527.
12. G.W. Goward, "Progress in Coatings for Gas Turbine Airfoils," Surface and Coatings Technology, V 108–109, 1998, pp. 73–79
13. G. Kappmeyer, C. Hubig, M. Hardy, M. Witty, M. Busch, "Modern Machining of Advanced Aerospace Alloys – Enabler for Quality and Performance," 5th CIRP Conference on High Performance Cutting 2012, Elsevier B.V., Amsterdam, The Netherlands, 2012, pp. 28–43.
14. P.S. Prevéy "X-Ray Diffraction Characterization of Residual Stresses Produced by Shot Peening," Shot Peening Theory and Application, ed. A. Niku-Lari, IITT-International, Gournay-Sur-Marne, France, 1990, pp. 81–93.
15. M.K. Tufft, "Shot Peen Impact on Life, Part 1: Development of a Fracture Mechanics/Threshold Behavior Predictive Model," Shot Peening Present & Future, Proc. of the 7th International Conference on Shot Peening, Institute of Precision Mechanics, 1999, pp. 244–253.
16. T.P. Gabb, R.A. Miller, C.K. Sudbrack, S.L. Draper, J.A. Nesbitt, R.B. Rogers, J. Telesman, V. Ngo, J. Healy, "Cyclic Oxidation and Hot Corrosion of NiCrY-Coated Disk Superalloys," NASA/TM—2016-219105, Washington, D.C., June, 2016.
17. J.T. Cammet, P.S. Prevéy, N. Jayaraman, "The Effect of Shot Peening Coverage on Residual Stress, Cold Work, and Fatigue in a Nickel-Base Superalloy," Proceedings of ICSP 9, 2005.
18. C.W. Bale, E. Bélisle, P. Chartrand, S.A. Decterov, G. Eriksson, A.E. Gheribi, K. Hack, I.-H. Jung, Y.-B. Kang, J. Melançon, A.D. Pelton, S. Petersen, C. Robelin, J. Sangster, P. Spencer, M-A. VanEnde, "FactSage Thermochemical Software and Databases, 2010–2016," CALPHAD: Computer Coupling of Phase Diagrams and Thermochemistry, V. 54, 2016, pp. 35–53.
19. Phase Equilibria Diagrams, in CD-ROM Database, Version 3.3.0, T.A.C.S. (ACerS), Editor. 2010, The American Ceramic Society (ACerS), 600 N. Cleveland Ave., Suite 210, Westerville, Ohio 43082.
20. J. Nesbitt, S.L. Draper, "Pit Morphology and Depth After Low-temperature Hot Corrosion of a Disc Alloy," Mat. at High Temperatures, V. 51 (4–5), 2016, pp. 501–516.

21. T.P. Ryan, Modern Experimental Design, John Wiley & Sons, Hoboken, New Jersey, 2007, pp. 169–179.
22. T.P. Gabb, R.B. Rogers, J.A. Nesbitt, R.A. Miller, B.J. Puleo, D. Johnson, J. Telesman, S.L. Draper, I.E. Locci, "Influences of Processing and Fatigue Cycling on Residual Stresses in a NiCrY-Coated Powder Metallurgy Disk Superalloy," J. of Materials Engineering and Performance, V. 26(11), 2017, pp. 5237–5250.
23. N. Bala, H. Singh, S. Prakash, "X-ray Diffraction Study of Cold Sprayed Ni-20Cr and Ni-50Cr Coatings on Boiler," Advanced Materials Research, V. 620, 2013, pp. 257–262.
24. J.F. Loersch, J.W. Neal, "Peened Overlay Coatings," U. S. 4,514,469, U. S. Patent Office, Washington, DC, 1985.
25. B.T. Hazel, M.J. Weimer, "Turbine Component Protected With Environmental Coating," U. S. 7,364,801 B1, U. S. Patent Office, Washington, DC, 2008.
26. K.L. Luthra, D.A. Shores, "Mechanism of Na_2SO_4 Induced Corrosion at 600 °C – 900 °C," Journal of the Electrochemical Society, V. 127(10), 1980, pp. 2202–2210.
27. D.R. Chang, D.D. Krueger, R.A. Sprague, "Superalloy Powder Processing, Properties and Turbine Disk Applications," Superalloys 1984, ed. M. Gell, C.S. Kortovich, R.H. Bricknell, W.B. Kent, J.F. Radavich, The Minerals, Metals & Materials Society, Warrendale, PA, 1984, pp. 245–273.